SAND2018-10785J

This paper describes objective technical results and analysis. Any subjective views or opinions that might be expressed in the paper do not necessarily represent the views of the U.S. Department of Energy or the United States Government

Study of the impact of resonant magnetic perturbation fields on gross tungsten erosion using DiMES samples in DIII-D

E.T. Hinson[a], O. Schmitz[a], H. Frerichs[a], T. Abrams[b], A. Briesemeister[c], D.L. Rudakov[d], E.A. Unterberg[c], W.R. Wampler[e], J.G. Watkins[e], H.Q. Wang[e]
[a]University of Wisconsin, Madison, WI 53706, USA
[b]General Atomics, P. O. Box 85608, San Diego, CA 92186-5608, USA
[c]Oak Ridge National Laboratory, Oak Ridge, TN, 37830, USA
[d]University of California (San Diego), La Jolla, USA
[e]Sandia National Laboratory, Albuquerque, NM

E-mail: hinsone@fusion.gat.com

Abstract. An experiment was conducted in DIII-D to compare gross tungsten (W) erosion on samples exposed to outer strike point (OSP) sweeps in L-mode plasmas for three conditions. These included two phases of resonant magnetic perturbations (RMPs), and a set with no perturbations. Upon RMP application, lobe structures indicative of strike point splitting of the OSP were evident in divertor camera data and on Langmuir probes. Gross W erosion, inferred spectroscopically using the S/XB method applied to the 400.9nm W-I line, was increased in the RMP cases by no more than 30% of the level observed in unperturbed discharges. A large reduction in gross erosion (50%) was observed in the private flux region (PFR) at the W sample for one specific toroidal phase of the RMP field.

1. Introduction

One of the challenges faced by ITER is mitigation of the damaging effects of plasma-material interactions (PMI) [1]. Edge Localized Modes (ELMs), a characteristic instability of H-mode plasmas, promptly expel edge plasma, and so have the potential to seriously damage plasma facing components after just a few 'type I' ELM events in a device the size of ITER [2]. One of the most promising of a variety of schemes to suppress ELMs is through the addition of small 3-D resonant magnetic perturbations (RMPs) to the applied axisymmetric confinement fields [3]. However, application of RMP fields perturbs the axisymmetric divertor footprint and generates a 3-D plasma boundary [4]. The 3-D boundary for the experiment in this paper is depicted in Figure **1**a, which shows the result from a field line following calculation. For that calculation, 3-D RMP fields were added to the axisymmetric field - the so-called 'vacuum approximation.' In actual experiments, corrections due to the plasma response are known to further modify this structure, even in L-mode [5].

When RMPs are applied, the strike point splits into separatrix lobes which are incident on the divertor as individual helical finger-like structures, formed from regions of plasma transported from the hot interior confined region [6]. Figure 1b shows a typical example of this modulation of heat flux as calculated with the 3-D code EMC3-EIRENE. How the application of these perturbations could be applied in ITER and beyond depends on their interaction with the material surfaces of those devices, which are currently envisaged to be constructed from tungsten (W) due to its sputter resistance and heat flux handling capability [7]. Strongly non-uniform erosion would necessitate either more frequent replacement of PFCs or spreading of the erosion

Sandia National Laboratories is a multimission laboratory managed and operated by National Technology & Engineering Solutions of Sandia, LLC, a wholly owned subsidiary of Honeywell International Inc., for the U.S. Department of Energy's National Nuclear Security Administration under contract DE-NA0003525

by, for instance, rotating the RMP fields, increasing coil stresses and thermal cycling of the cooling bonds in the divertor [2].

Only a few studies have been done to date to examine the impact of RMP ELM suppression on the integrity of plasma facing components (PFCs). Previous work in DIII-D [8] has shown that chemical erosion yields can be altered significantly within the helical lobes. The present experiment extends this discussion by investigating physical sputtering-induced erosion of W PFCs through a comparison of cases with and without exposure to RMP.

2. Experiment

DIII-D is a 1.67 m major radius tokamak with minor radius of 0.67 m with ATJ™ graphite plasma facing surfaces. Figure 1a shows a cross-section of the divertor region of DIII-D and the diagnostics used in this study for characterization of PMI at the outer strike point (OSP).

The Divertor Material Evaluation System (DiMES) [9] is an experimental system on the divertor shelf in DIII-D capable of between-discharge exchange of samples for exposure to the OSP plasma. For this work, the DiMES manipulator, at $\mathbf{R}_{DiMES}$ = 1.485 m, was loaded with 5 cm diameter ATJ graphite sample substrates that were coated with 40nm of magnetron-sputtered W at Sandia National Laboratory.

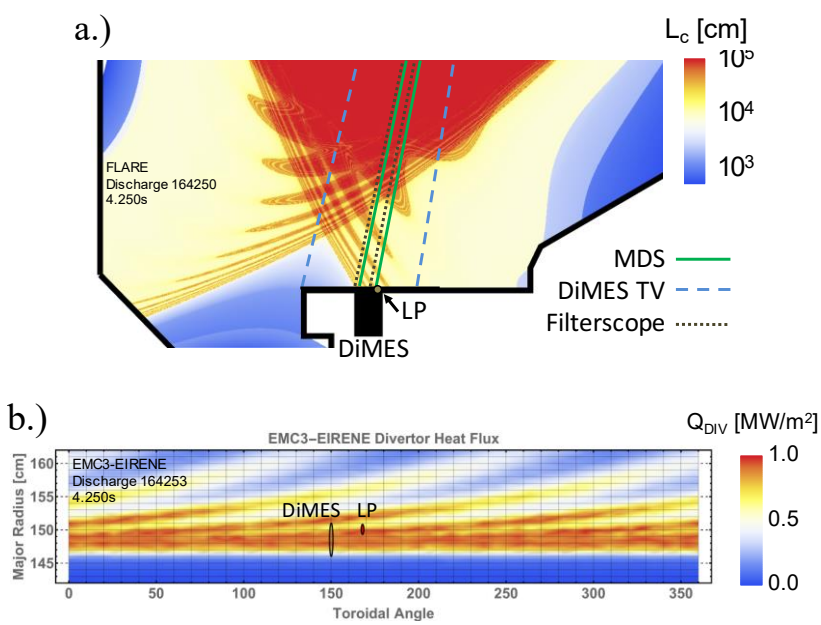

Figure 1: a.) Cross-section of the DIII-D tokamak divertor region, including an example connection length (L_c) plot of a discharge from this work, and the DiMES diagnostic suite's OSP access. b.) Heat flux plot example showing modulated heat flux pattern due to RMP applications obtained with EMC3-EIRENE.

The DiMES diagnostic suite includes, among other diagnostics, floor Langmuir probes (LPs) located $\Delta \quad = 18°$ toroidally away at $\quad = 1.50$ m, a multichord divertor spectrometer (MDS) [10] with a 3 cm diameter viewing chord centered on the DiMES sample, a divertor filtered camera (DiMES TV) [11], and a filtered photomultiplier, or filterscope [12], with a 2.5 cm diameter view onto DiMES. These diagnostics and their relation to the OSP are shown in Figure 1. Figure 2 shows a typical image taken from DiMES TV, centered on the W sample, during a discharge from this work. The filterscope view spot is indicated. The radial and downfield direction are also shown. The circular mask is the result of a vignetting correction.

The internal magnetic perturbation coils (I-coils) at DIII-D are capable of adding a toroidal mode number n=3 perturbation to the usual, nominally axisymmetric, magnetic configuration. They were operated for this experiment in the up-down symmetric 'even configuration' where polarity of the coil current alternates only in the toroidal orientation. This allows for 2 phase configurations corresponding to a 60 degree toroidal rotation of the perturbation. The so-called '60 degree' and '0 degree' configurations were both used, with a current of 3.9kA and allow placement of the DiMES sample at two positions in the helical magnetic footprint. [3]

To avoid the contaminating effect of ELM-induced erosion in H-mode, and because RMP-ELM suppression cannot be guaranteed with the OSP on the divertor shelf, the experiment was conducted with lower single null (LSN) L-mode plasmas. The discharges under consideration had the following parameters: separatrix density $n_{e,sep}$=5x10^{19} m^{-3}, and input/radiated power P_{input}=1.8 MW, and P_{rad}=1.0MW. At the OSP, LP measurements of electron temperature were T_e = 20-30 eV, so overall W erosion level was low.

The samples were exposed to a wide region of scrape off layer (SOL) and private flux region (PFR). The OSP was swept across DiMES, from 1.42 m, to 1.53 m, and back to 1.42 m, over 1.3 s in each direction. Three different magnetic configurations were used – 60 degrees for both sweeps (2 discharges), 60 degrees for the sweep out switching to 0 for the sweep back in (2 discharges), and a set with no RMPs (6 discharges).

Gross W erosion was measured using the S/XB method applied to the 400.9nm line of neutral tungsten [13], [14]. The S/XB coefficient converts light emission into particle fluxes by quantifying the ionization to line emission intensity ratio. When all neutral W originates from the surface, the S/XB coefficient gives the atomic flux Γ_{W-I} from the surface per unit photon flux. The S/XB coefficient depends on the local T_e and n_e, and was adjusted according to the plasma conditions determined by the probe at 1.50 m. The relatively quiescent L-mode conditions of the experiment were in this respect an advantage as the intermittent ELM-induced erosion risk could be avoided. Line intensities and background continuum were measured with a spectrometer tuned to a range around the 400.9nm line. This was used to calibrate the DiMES-viewing filterscope, which was equipped with a 2 nm bandpass filter around 400.9nm, and the a divertor camera, which was equipped with a 1.5nm bandpass filter about 400.9nm.

3. Results and Analysis

The separatrix lobes are clearly visible in the images from the DiMES TV. In Figure 2b images processed by difference filtration are shown, in which the leading and trailing frame were subtracted from twice the current frame:

$$\mathrm{Diff}[i] = 2\mathrm{Frame}[i] - \mathrm{Frame}[i-1] - \mathrm{Frame}[i+1]$$

removing static structures. Integrating pixel values in the toroidal direction and correcting for the geometric distortion due to the circular mask produces line profiles shown in Figure 2c. The ~1-2 cm radial features obtained appear upon application of RMP, and maintain a roughly consistent shape through the sweep. When RMP phase is flipped from 60 to 0 degrees after 3100 ms, the lobe pattern is observed to obtain opposite phase in the SOL – consistent expectation for a ½ period toroidal shift of a purely n = 3 perturbation. The profiles are aligned in Figure 2c so that the OSPs, determined with EFIT equilibrium reconstructions [15], coincide.

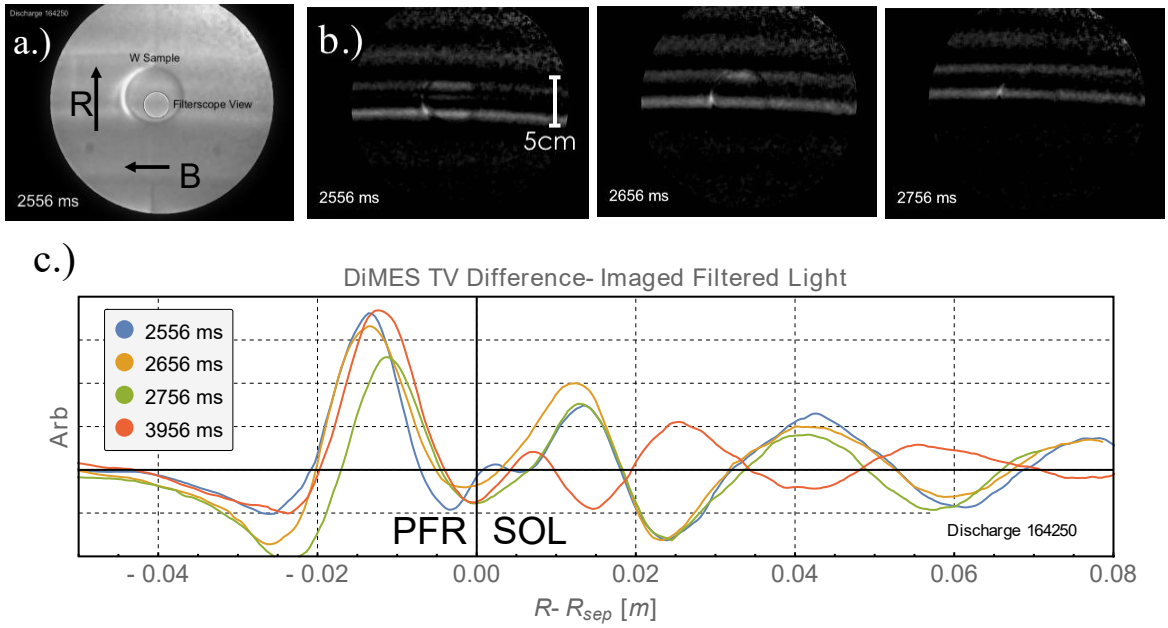

Figure 2: a.) Image from DiMES TV, with a framerate of 10Hz, during a shot. The tungsten sample and filterscope view are indicated. b.) Difference filtration of DiMES TV imaging, showing motion of separatrix lobes that appear upon RMP application. c.) Line profiles taken from difference imaging, exhibiting consistent structure during each sweep.

The modulated plasma characteristic of separatrix lobes was also observed with Langmuir probes [16]. Probe data vs OSP position from the probe at R=1.50 m is shown in Figure 3. For the no-RMP case, $\mathbf{T}_e$ was higher for the sweep inward than for the initial outward sweep. Modulations, particularly in the measured floating potential, exist between no-RMP and RMP cases. Modulations in $\mathbf{n}_e$ and $\mathbf{T}_e$ are more subtle and approach the level of noise. The $\mathbf{V}_{float}$ profiles and the divertor camera images confirm the creation of separatrix lobes in L-mode.

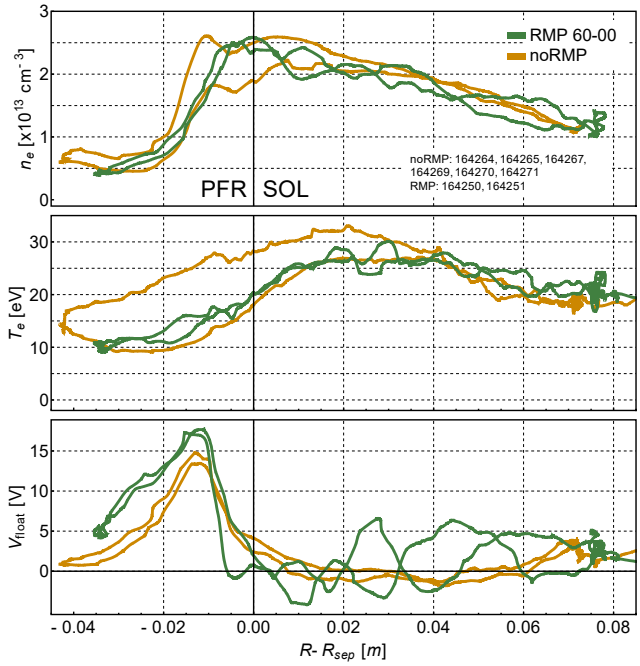

Figure 3: LP traces of plasma parameters for the noRMP and RMP 60 deg/0 deg cases. Lobe-related modulations are visible for the RMP sweeps.

An absolutely-calibrated multi-chord divertor spectrometer (MDS) was used to measure the 400.9 nm W-I line and nearby continuum with 2 Hz. In Figure 4a, the time-integrated spectrum for 12 shots with the spectrometer tuned to this spectral range is shown, corresponding to 1.2 minutes of total exposure. The integrated spectrum was used to determine peak locations and widths. Those parameters were subsequently held constant for fitting the individual time-resolved spectra, where only peak amplitudes and background continuum level was fitted, with their standard error for propagation in subsequent analysis. An example fit is shown in Figure 4b. The two fits to the W-I line indicate the +/- standard error for this fit.

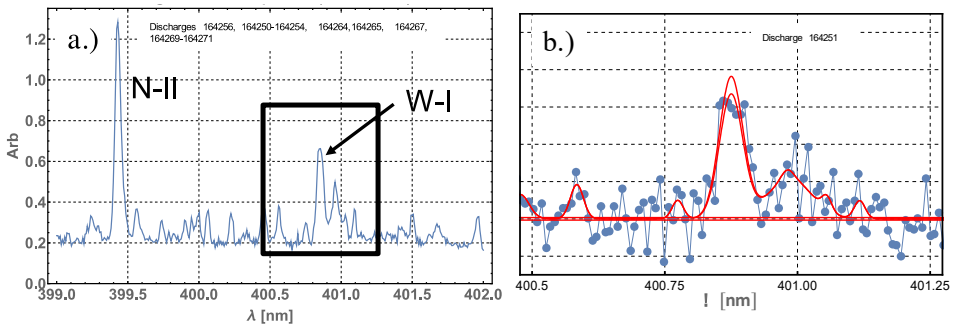

Figure 4: a.) Integrated spectrometer time record. b.) Zoom to region of fitted spectrum at W-I line.

The 3 cm diameter of the MDS view chord spot is not favorable for measuring an erosion pattern having features with sizes shown in Figure 2 and Figure 3. Additionally, because spectra are taken at 2 Hz, and the structures traverse the spot at ~8cm/s, (4 cm/exposure) each exposure of the spectrometer integrates over the lobe structure in time and space. Thus, the MDS integrates over modulations that might be expected from the lobes and tends to wash out the modulated W-I emission. While time-resolved measurements of individual modulations are not expected, time-integrated gross erosion over the entire set of discharges can be estimated, and totals 3 nm for both the RMP and no-RMP samples (with 10 exposure to each sample). This is an upper bound on net erosion, which agrees with the value from ex-situ measurements using RBS of < 1 nm, the detection limit for that technique [17].

The spectrometer can be used to determine the ratio of the W-I line to background continuum, enabling calibration of filtered diagnostics with higher time resolution [18]. After calibration, the filterscope and DiMES TV provide a higher-frequency measurement of the W-I emission [11]. Calibrations for times between MDS time points were linearly interpolated. Standard error from MDS fits was propagated to this calibration factor, and then to the W-I measurements, where it is presumed to be the dominant measurement uncertainty.

The calibrated W-I light was multiplied by the time-evolving S/XB coefficient to produce erosion rates from the filterscope and DiMES TV data. Percent change in erosion measured for the RMP case vs the no RMP case, computed as

$$\Delta(t) = 100\,\frac{\Gamma_{W-I,RMP}(t) - \Gamma_{W-I,noRMP}(t)}{\Gamma_{W-I,noRMP}(t)} \qquad [1]$$

was found as a function of distance between the OSP location $\mathbf{R}_{OSP}$ and filterscope spot center $\mathbf{R}_{FSspot}$ for both diagnostics. The data for the 60 degree sweep out was combined for both the 60-00 sweeps and 60-60 sweeps into a single set for better statistics. Results from the filterscopes with propagated error is shown in Figure 5 as a shaded region.

DiMES TV data within the region of the filterscope view spot was used to calculate erosion. In contrast to the filterscope, which integrates over its spot, the higher spatial resolution

of DiMES TV can produce radial profiles of erosion difference, Δ, at each frame after toroidal averaging. Additionally, for comparison, the filterscope measurement was replicated by averaging DiMES data over the entire filterscope spot. The results are shown in Figure 5a and b. Dots represent Δ after averaging camera data over the spot. Corresponding radial profiles of Δ can be seen running through each dot. These profiles indicate measurement precision, and adjacent frames give the same result for the same location vs the OSP mostly to within ~10%, though with exceptions. The profiles suggest the 2.5 cm filterscope spot size is sufficient for measurements with OSP sweeps.

Lastly, Figure 5 includes difference-imaged DiMES TV data, to facilitate comparison of erosion to lobe structures. Because there is minor change in the lobes over the sweep, only difference imaging from the region within the filterscope spot is shown. Each frame contributes a 2.5 cm section, and a lobe profile as seen at $\mathbf{R}_{FSspot}$ is generated.

The magnitude of erosion modulations in Figure 5 is generally less than 30% of the unperturbed value, and broad agreement exists between the divertor camera and filterscope measurements. Further, while the divertor camera in particular has the capability to resolve much smaller structures, the size scale of oscillations is not smaller than the characteristic scale of the lobes identified with difference imaging and LPs.

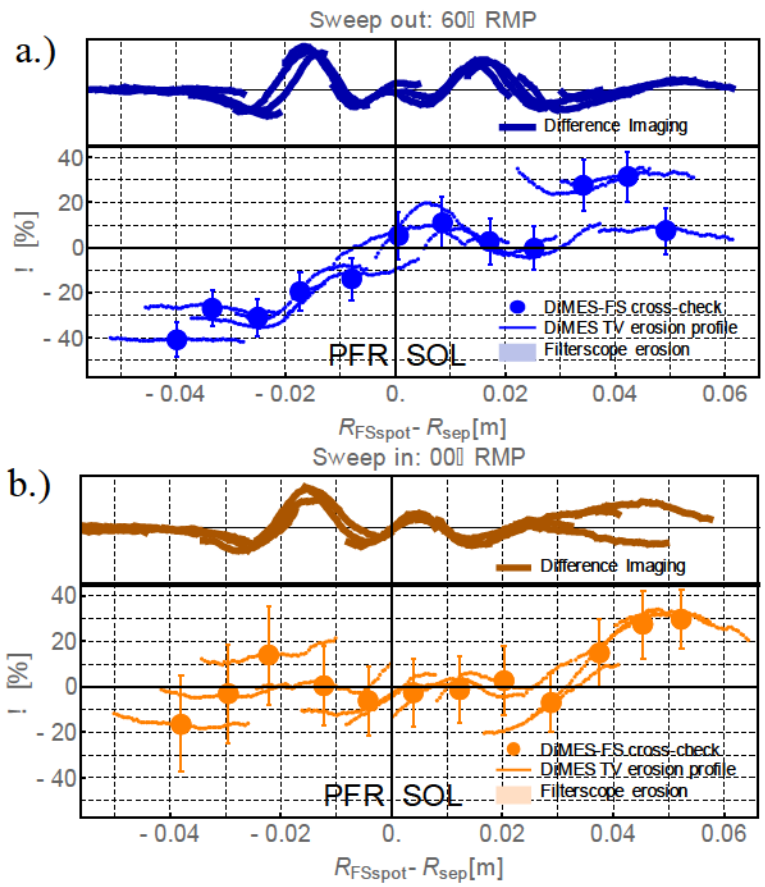

Figure 5: Percent difference in erosion Δ with DiMES TV and filterscopes for the sweep out, a.), and the sweep back in, b.). The shaded regions correspond to the filterscope measurement. The dots show Δ from DiMES TV data averaged over the entire filterscope spot. Radial profiles of Δ extend about either side of the average value. Difference imaging of light over the filterscope spot is shown as heavy dark curve segments.

4. Discussion

In discharges with RMP, modulations characteristic of separatrix lobes during strike point sweeps were evident on probe traces and in difference-imaging of light from a filtered divertor camera. Features were ~2 cm in size.

Gross erosion changes due to RMP were limited to low 10s of percent of the unperturbed gross erosion rate for the conditions in this work, which was near 0.1nm/s at the OSP. Inferred gross erosion data possesses features at similar wavenumbers to the lobes, despite higher wavenumber features being resolvable. Better statistics would be required to establish a precise correspondence between the lobes and these features.

There was a statistically significant reduction in gross erosion measured in the PFR, which reached ~ 50% of the unperturbed value at DiMES in the 60-degree phase. Likewise, increased erosion during RMP was measured in the far SOL, particularly for the 0-degree phase. While RMP application may have global effects on erosion not depending on phase, the phase angle dependence observed in the largest effects on erosion is consistent with a substantially 3-D impact.

Future work should operate in RMP ELM-suppressed H-mode, where closer approximation to ITER conditions are obtained, and higher W-I emission will allow more precise quantification of RMP erosion effects. The ~ 50% upper limit to changes in the PFR and SOL found in this L-mode study may be set by its low ion energies and resulting W physical sputtering rates. In H-mode conditions, the ion energy will substantially exceed the W sputtering threshold and a stronger impact of the features observed here could exist.

5. Acknowledgements

This material is based upon work supported by the U.S. Department of Energy, Office of Science, Office of Fusion Energy Sciences, using the DIII-D National Fusion Facility, a DOE Office of Science user facility, under Awards DE-FC02-04ER54698. Work also supported by US DOE DE-SC0013911, DE-AC05-06OR23100, DE-FG02-07ER54917, DE-AC05-00OR22725, and DE-AC04-94AL85000. DIII-D data shown in this paper can be obtained in digital format by following the links at https://fusion.gat.com/global/D3D_DMP.

6. References

[1] G. Federici, et al., "Plasma-material interactions in current tokamaks and their implications for next step fusion reactors," **Nud. Fusion**, vol. 41, no. 12, pp. 1967–2137, Dec. 2001.

[2] A. Loarte, et al., "Progress on the application of ELM control schemes to ITER scenarios from the non-active phase to DT operation," **Nud. Fusion**, vol. 54, no. 3, p. 33007, Mar. 2014.

[3] T. E. Evans, et al., "Edge stability and transport control with resonant magnetic perturbations in collisionless tokamak plasmas," **Nat. Phys.**, vol. 2, no. 6, pp. 419–423, Jun. 2006.

[4] O. Schmitz, et al., "Three-dimensional modeling of plasma edge transport and divertor fluxes during application of resonant magnetic perturbations on ITER," **Nud. Fusion**, vol. 56, no. 6, p. 66008, Jun. 2016.

[5] O. Schmitz, et al., "Formation of a three-dimensional plasma boundary after decay of the plasma response to resonant magnetic perturbation fields," **Nud. Fusion**, vol. 54, no. 1, p. 12001, Jan. 2014.

[6] M. W. Jakubowski, et al., "Overview of the results on divertor heat loads in RMP controlled H-mode plasmas on DIII-D," **Nucl. Fusion**, vol. 49, no. 9, p. 95013, Sep. 2009.
[7] R. Neu, et al., "Preparing the scientific basis for an all metal ITER," **Plasma Phys. Control. Fusion**, vol. 53, no. 12, p. 124040, Dec. 2011.
[8] O. Schmitz, et al., "The influence of three-dimensional stochastic magnetic boundaries on plasma edge transport and the resulting plasma wall interaction," **J. Nucl. Mater.**, vol. 415, no. 1, pp. S886–S893, 2011.
[9] C. P. C. Wong, et al., "Divertor materials evaluation system at DIII-D," **J. Nucl. Mater.**, vol. 196–198, pp. 871–875, Dec. 1992.
[10] N. H. Brooks, et al., "Multichord spectroscopy of the DIII-D divertor region," **Rev. Sci. Instrum.**, vol. 63, no. 10, pp. 5167–5169, Oct. 1992.
[11] T. Abrams, et al., "The inter-ELM tungsten erosion profile in DIII-D H-mode discharges and benchmarking with ERO+OEDGE modeling," **Nucl. Fusion**, vol. 57, no. 5, p. 56034, May 2017.
[12] R. J. Colchin, et al., "The Filterscope," **Rev. Sci. Instrum.**, vol. 74, no. 3, pp. 2068–2070, Mar. 2003.
[13] H. P. Summers, "The ADAS User Manual," 2004. [Online]. Available: http://www.adas.ac.uk.
[14] S. Brezinsek, "The JET-ILW and Plasma Edge Spectroscopy in Metallic Fusion Devices," in **18th International Conference on Atomic Processes in Plasmas**, 2013.
[15] L. L. Lao, et al., "Equilibrium analysis of current profiles in tokamaks," **Nucl. Fusion**, vol. 30, no. 6, pp. 1035–1049, Jun. 1990.
[16] D. Buchenauer, et al., "Divertor plasma characterization using Langmuir probes in DIII-D," **J. Nucl. Mater.**, vol. 176–177, pp. 528–532, Dec. 1990.
[17] D. L. Rudakov, et al., "Net versus gross erosion of high- Z materials in the divertor of DIII-D," **Phys. Sc.**, vol. T159, no. T159, p. 14030, Apr. 2014.
[18] N. Den Harder, et al., "ELM-resolved divertor erosion in the JET ITER-Like Wall," **Nucl. Fusion**, vol. 56, no. 2, p. 26014, Feb. 2016.